

# Effect of Doping on the phase stability and Superconductivity in LaH<sub>10</sub>

Zepeng Wu<sup>1</sup>, Yang Sun<sup>1\*</sup>, Feng Zheng<sup>1</sup>, Vladimir Antropov<sup>2,3</sup>, Kai-Ming Ho<sup>3</sup>, Shunqing Wu<sup>1\*</sup>

<sup>1</sup>*Department of Physics, Xiamen University, Xiamen 361005, China*

<sup>2</sup>*Ames National Laboratory, Ames, Iowa 50011, USA*

<sup>3</sup>*Department of Physics, Iowa State University, Ames, Iowa 50011, USA*

## Abstract

We present a computational investigation into the effects of chemical doping with 15 different elements on phase stability and superconductivity in the LaH<sub>10</sub> structure. Most doping elements were found to induce softening of phonon modes, enhancing electron-phonon coupling and improving critical superconducting temperature while weakening dynamical stability. Unlike these dopants, Ce was found to extend the range of dynamical stability for LaH<sub>10</sub> by eliminating the van Hove singularity near the Fermi level. The doped compound, La<sub>0.75</sub>Ce<sub>0.25</sub>H<sub>10</sub>, maintains high-temperature superconductivity. We also demonstrate that different Ce doping configurations in the LaH<sub>10</sub> structure have a minimal effect on energetic stability and electron-phonon coupling strength. Our findings suggest that Ce is a promising dopant to stabilize LaH<sub>10</sub> at lower pressures while preserving its high-temperature superconductivity.

---

<sup>1</sup> Email: [yangsun@xmu.edu.cn](mailto:yangsun@xmu.edu.cn) (Y.S.) and [wsq@xmu.edu.cn](mailto:wsq@xmu.edu.cn) (S.W.)

1   **I. INTRODUCTION**

2   In recent years, it has been experimentally observed that H-rich compounds can exhibit high-  
3   temperature superconductivity (HTS) under high pressure, such as H<sub>3</sub>S ( $T_c = 203\text{K}$  at 155GPa [1]),  
4   LaH<sub>10</sub> (250K at 188GPa [2,3]), CaH<sub>6</sub> (215K at 172GPa [4,5]), CeH<sub>10</sub> (115K at 95GPa [6]), CeH<sub>9</sub>  
5   (~100K at 130GPa [6]), (LaCe)H<sub>9</sub> (148-178K at 97-172GPa [7,8]), YH<sub>9</sub> (243K at 201GPa [9-11]),  
6   YH<sub>6</sub> (~220K at 183GPa [9]), and LaBeH<sub>8</sub> (110K at 80GPa [12]). These discoveries have set a  
7   milestone in approaching the room-temperature superconductivity [13-18]. At the same time, the  
8   pressure required to stabilize these compounds is still too extreme for practical applications.

9   The search of binary hydrides [19,20] has shown diverse structures and chemistry in these  
10   compounds, which provide a wide platform to optimize the energetic stability and superconductivities.  
11   Compared with the binary phases, the ternary phases have a much broader configurational space and  
12   provide more possibility for HTS at lower pressures [21]. Recently it has been proposed that replacing  
13   H with small-radius elements (such as Be, B, C, N, and Si) can lower the required high pressures in  
14   the hydrides [22]. For instance, KB<sub>2</sub>H<sub>8</sub> (134K-146K at 12GPa [23]), BaSiH<sub>8</sub> (71K at 3GPa [24]),  
15   LaBH<sub>8</sub> (126K at 50GPa [25]), KPb(BC)<sub>6</sub> (88K at ambient pressure [26]), Al<sub>2</sub>(BN)<sub>6</sub> (72K at ambient  
16   pressure [27]), etc. While these dopants extend the pressure range of the stability, their superconducting  
17   temperature is simultaneously reduced.

18   Since the superconductivity in hydrides is mainly due to H, doping on the metal site is likely to  
19   maintain its superconductivity. Recently high-throughput screening in the MgB<sub>2</sub>-like systems shows  
20   that the doping on the metal site can effectively improve the stability and even maintain a  
21   superconductivity [28]. Metals from the same family share characteristics that can be combined into  
22   disordered solid mixtures. This property allows us to use binary compounds as foundational blueprints  
23   for crafting ternary alloy super hydrides from the original crystal structure [29-32]. LaH<sub>10</sub>, with the  
24   highest  $T_c$  among experimentally synthesized superconductors, is a potential parent structure for  
25   doping to manipulate its HTS and pressure-dependent stability.

26   In this paper, based on first-principles calculations, we investigate the effects of chemical doping  
27   on phase stability and superconductivity in the LaH<sub>10</sub> structure. A total of 15 elements are selected as  
28   dopants: K, Rb, Cs, Ca, Sr, Ba, Sc, Y, Ti, Zr, Hf, In, Tl, Ce, and Lu. The first thirteen elements are  
29   more likely to donate electrons to H atoms to enhance the stability of the H cage framework, and the  
30   strong correlation effect caused by  $d$  electrons is not significant [20]. Ce and Lu have also been  
31   theoretically predicted to have good superconducting potential [33,34]. We will use the La<sub>0.75</sub>M<sub>0.25</sub>H<sub>10</sub>  
32   model to examine their dynamical stability and superconductivity under high pressure.

33 **II. COMPUTATION METHODS**

34 The La<sub>0.75</sub>M<sub>0.25</sub>H<sub>10</sub> structure is constructed by replacing one La atom with M metal (M=K, Rb,  
 35 Cs, Ca, Sr, Ba, Sc, Y, Ti, Zr, Hf, Ce, Lu, In, Tl) in the conventional cell (four formula units (f.u.))  
 36 shown in Fig. 1(a). This results in a symmetry reduction to Pm-3m. Structure relaxations and electronic  
 37 properties were carried out using the Perdew-Burke-Ernzerhof (PBE) [35] functional in the framework  
 38 of the projector augmented wave (PAW) method [36] as implemented in the VASP code [37]. The  
 39 configurations of valence electrons used in the PAW method are shown for these elements in Table.  
 40 S1. A plane-wave basis set with an energy cutoff of 500 eV and uniform  $\Gamma$ -centered k-point grids with  
 41 a density of  $2\pi \times 0.025\text{\AA}^{-1}$  was employed in the self-consistent calculations and structure  
 42 relaxations. The structures were optimized until the maximum energy and force were less than  
 43  $10^{-8}$  eV and 1 meV/ $\text{\AA}$ , respectively.

44 Harmonic phonon dispersion and electron-phonon coupling (EPC) were calculated within the  
 45 density functional perturbation theory (DFPT) [38], as implemented in the QUANTUM ESPRESSO  
 46 package [39,40]. Ultrasoft pseudopotentials [41] with PBE functional were used with a kinetic energy  
 47 cutoff of 80 Ry and a charge density cutoff of 800 Ry. The valence electron configurations used in  
 48 USPP were the same as in PAW potential, so the calculations performed with QE and VASP were  
 49 consistent. Self-consistent electron density and EPC were calculated by employing  $8\times 8\times 8$   $k$ -point  
 50 meshes and  $4\times 4\times 4$   $q$ -point meshes. A dense  $16\times 16\times 16$   $k$ -point mesh was used for evaluating an  
 51 accurate electron-phonon interaction matrix.

52 The calculations of superconducting temperature  $T_c$  are based on the Eliashberg spectral  
 53 equation  $\alpha^2 F(\omega)$  defined as[42,43]

$$54 \quad \alpha^2 F(\omega) = \frac{1}{2\pi N(E_F)} \sum_{qv} \frac{\gamma_{qv}}{\hbar\omega_{qv}} \delta(\omega - \omega_{qv}), \quad (1)$$

55 where  $N(E_F)$  is the states at the Fermi level  $E_F$ ,  $\omega_{qv}$  representative the phonon frequency of the  
 56 mode  $v$  with wave vector  $q$ . The phonon linewidth  $\gamma_{qv}$ , which is the imaginary part of the phonon self-  
 57 energy, is defined as

$$58 \quad \gamma_{qv} = \frac{2\pi\omega_{qv}}{\Omega_{B,Z}} \sum_{i,j} \int d^3k |g_{k,qv}^{i,j}|^2 \delta(\varepsilon_{i,q} - E_F) \delta(\varepsilon_{j,k+q} - E_F), \quad (2)$$

59  $g_{k,qv}^{i,j}$  is the EPC matrix element, and  $\Omega_{B,Z}$  is the volume of the Brillouin zone (B.Z.).The EPC  
 60 constant is calculated by

$$61 \quad \lambda = \sum_{qv} \frac{\gamma_{qv}}{\pi\hbar N(E_F)\omega_{qv}^2} = 2 \int_0^\infty \frac{\alpha^2 F(\omega)}{\omega} d\omega. \quad (3)$$

62  $T_c$  is obtained by the McMillan-Allen-Dynes formula [42,43] with Coulomb pseudopotential  $\mu^* =$   
 63 0.13 [44,45].

$$T_c = \frac{f_1 f_2 \omega_{log}}{1.2} \exp\left(-\frac{1.04(1+\lambda)}{\lambda - \mu^*(1+0.62\lambda)}\right), \quad (4)$$

where  $f_1$  and  $f_2$  are two separate correction factors [42], which are functions of  $\lambda$ ,  $\omega_{log}$ ,  $\omega_2$ , and  $\mu^*$ . The logarithmic average frequency  $\omega_{log}$  is computed as  $\omega_{log} = \exp\left(\frac{2}{\lambda} \int_0^\infty \frac{\alpha^2 F(\omega)}{\omega} \ln \omega d\omega\right)$ .

### III. RESULTS AND DISCUSSION

#### 3.1 Phase stability

We first evaluate the dynamical stability of ternary  $\text{La}_{0.75}\text{M}_{0.25}\text{H}_{10}$  structures. Harmonic phonon dispersions were calculated for all 16 phases at 400GPa, 250GPa, and 200GPa (see Supplementary Fig. S1). The phase without any imaginary modes in the phonon spectrum is marked as dynamically stable. The data are summarized in Fig. 1(b). At 400 GPa, the structure is stable with seven substitutions, i.e., Sr, Ba, Y, Zr, Hf, Ce, and Lu. Y and Ce substitutions can maintain stability when the pressure is reduced to 250 GPa. At 200 GPa, only  $\text{La}_{0.75}\text{Ce}_{0.25}\text{H}_{10}$  remains to be stable.  $\text{LaH}_{10}$  becomes dynamically unstable at 220 GPa (see Fig. S2). Therefore, Ce substitution can improve the stability of  $\text{LaH}_{10}$  and expand the pressure range of the stability. Our calculations are based on the harmonic approximation, and the anharmonic effect was ignored. Previous calculations with anharmonic correction indicate the  $\text{LaH}_{10}$  can be stabilized as low as  $\sim 130$  GPa [46], consistent with the experimental observation at  $\sim 140$  GPa [47]. The pressure stability range of  $\text{La}_{0.75}\text{Ce}_{0.25}\text{H}_{10}$  is expected to expand further by including anharmonic effects.

Given its dynamical stability, we also evaluate the thermodynamic stability of  $\text{La}_{0.75}\text{Ce}_{0.25}\text{H}_{10}$ . We calculated its enthalpy on the ternary phase diagram at 200 GPa, as shown in Fig. S3. The results show that the energy of the  $\text{La}_{0.75}\text{Ce}_{0.25}\text{H}_{10}$  structure is only 1 meV/atom higher than that of the convex hull, which indicates that the  $\text{La}_{0.75}\text{Ce}_{0.25}\text{H}_{10}$  has promising thermodynamic stability. Its synthesizable range is broader than  $\text{LaH}_{10}$ .

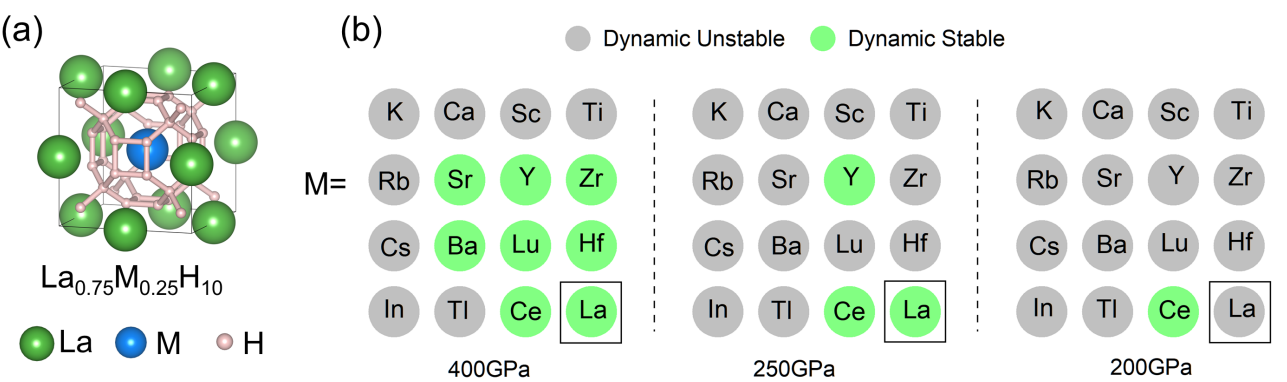
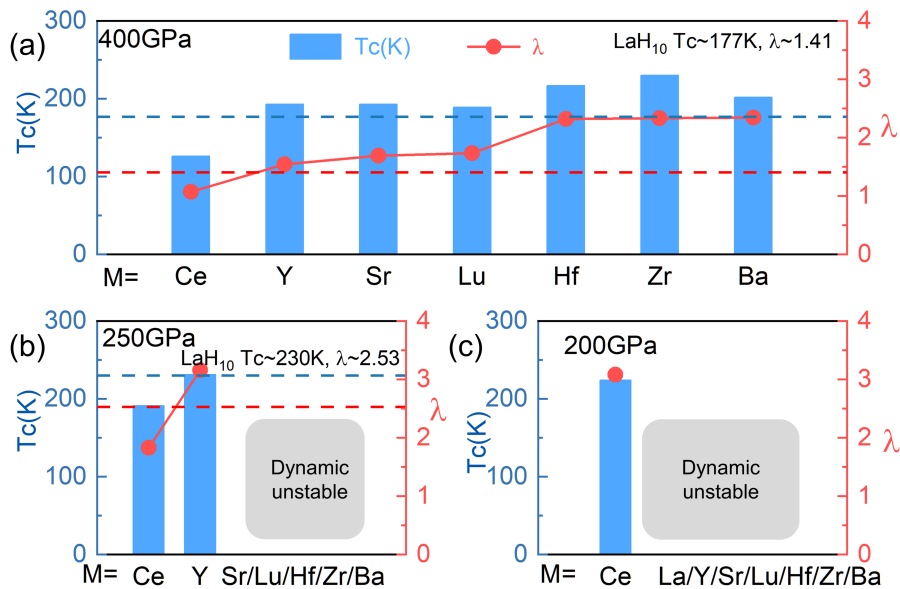


Fig. 1. (a) Structure of  $\text{La}_{0.75}\text{M}_{0.25}\text{H}_{10}$ ,  $\text{M}=\text{K}, \text{Rb}, \text{Cs}, \text{Ca}, \text{Sr}, \text{Ba}, \text{Sc}, \text{Y}, \text{La}, \text{Ti}, \text{Zr}, \text{Hf}, \text{In}, \text{Tl}, \text{Ce}, \text{Lu}$ . (b) Dynamic stability of all doped phases at 400 GPa, 250 GPa, and 200 GPa.

89 **3.2 Electron-phonon coupling and superconductivity**

90 For the dynamically stable structures, we calculate the EPC constant  $\lambda$  using the DFPT method and  
 91 Eliashberg theory, and the superconducting transition temperature ( $T_c$ ) by the McMillan-Allen-Dynes  
 92 formula, presented in Fig. 2. The calculation of  $\text{LaH}_{10}$  shows that  $\lambda$  is 2.53 and  $T_c$  is 230 K at 250  
 93 GPa. This result is consistent with previous calculations using the same formula in [44] ( $\lambda=2.29$  and  
 94  $T_c=212\text{K}$  at 250GPa). As a reference, the experimental  $T_c$  of  $\text{LaH}_{10}$  was observed at  $\sim 250\text{K}$  under  $\sim$   
 95 220GPa [2]. Therefore, our calculation of  $T_c$  is also comparable with the experimental data. In Fig.  
 96 2(a), we found that substitution with Y, Sr, Lu, Hf, Zr, and Ba all enhance the EPC constant and  $T_c$  at  
 97 400 GPa, while the substitution with Ce weakens them. Similarly, at 250 GPa,  $\lambda$  and  $T_c$  increase  
 98 with Y substitution while decreasing with Ce substitution. At 200 GPa, the only stable phase  
 99  $\text{La}_{0.75}\text{Ce}_{0.25}\text{H}_{10}$  remains a potential high- $T_c$  superconductor with  $T_c$  of 224 K and  $\lambda$  of 3.08.



100  
 101 Fig. 2. Superconducting transition temperature ( $T_c$ ) and electron-phonon coupling constant  $\lambda$  of stable  
 102  $\text{La}_{0.75}\text{M}_{0.25}\text{H}_{10}$  structures at (a) 400GPa, (b) 250GPa and (c) 200GPa

103 To understand the origin of the increased  $\lambda$  and  $T_c$  by doping, we use  $\text{La}_{0.75}\text{Hf}_{0.25}\text{H}_{10}$  as an  
 104 example and compare its phonon spectra to the  $\text{LaH}_{10}$  in Fig. 3. We find the substitution of La with Hf  
 105 induces significant softening of high-frequency phonon modes. As shown in Fig. 3(a), with the Hf  
 106 substitution, a few phonon modes appear in the low-frequency range of  $360\text{-}900\text{ cm}^{-1}$ , while no phonon  
 107 modes exist in the same area for  $\text{LaH}_{10}$ . The H atoms dominate these phonon modes (see the projected  
 108 phonon DOS in Fig. S4). Comparing the Eliashberg spectral function between  $\text{LaH}_{10}$  and  
 109  $\text{La}_{0.75}\text{Hf}_{0.25}\text{H}_{10}$  in Fig. 3 (b) and (c), one can see the phonon softening at the range of  $360\text{-}900\text{ cm}^{-1}$

significantly promotes the EPC in this region. Similar enhancement of phonon linewidth in 360-900 cm<sup>-1</sup> can be found by comparing Fig. 2 (d) and (e). If we integrate Eqn. (3) to  $\omega = 900\text{cm}^{-1}$ , we find the contribution to  $\lambda$  from frequencies less than 900cm<sup>-1</sup> is 0.18 and 1.01 for LaH<sub>10</sub> and La<sub>0.75</sub>Hf<sub>0.25</sub>H<sub>10</sub>, respectively. Therefore, the phonon softening in La<sub>0.75</sub>Hf<sub>0.25</sub>H<sub>10</sub> significantly enhances the EPC. This mechanism is also seen in other superconducting systems [48-51]. The analysis of La<sub>0.75</sub>Hf<sub>0.25</sub>H<sub>10</sub> illustrates that substituting La with Hf changes the bonding with H atoms and softens vibrational modes. Such phonon softening enhances the EPC and increases the  $\lambda$  and  $T_c$ , simultaneously. We also analyzed the EPC for other dopants and found similar effects, as shown in Fig. S4 and Table S2, i.e., the substitution of La leads to phonon softening, which contributes to strong EPC in the middle- and low-frequency regions.

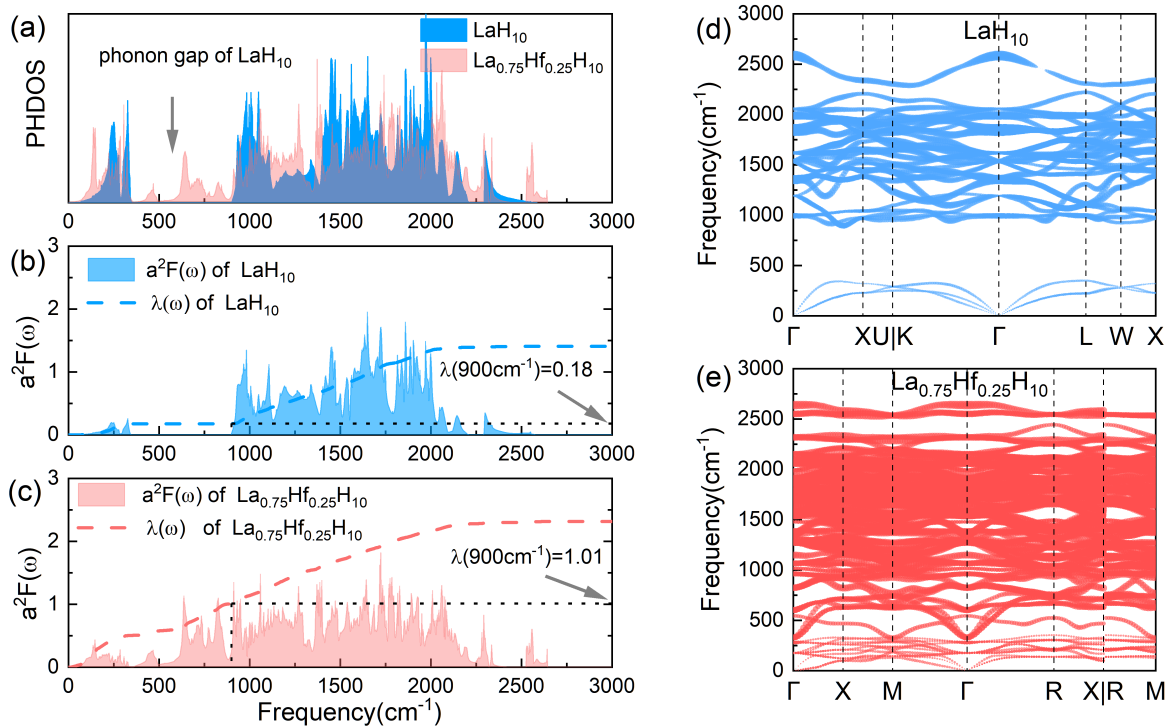
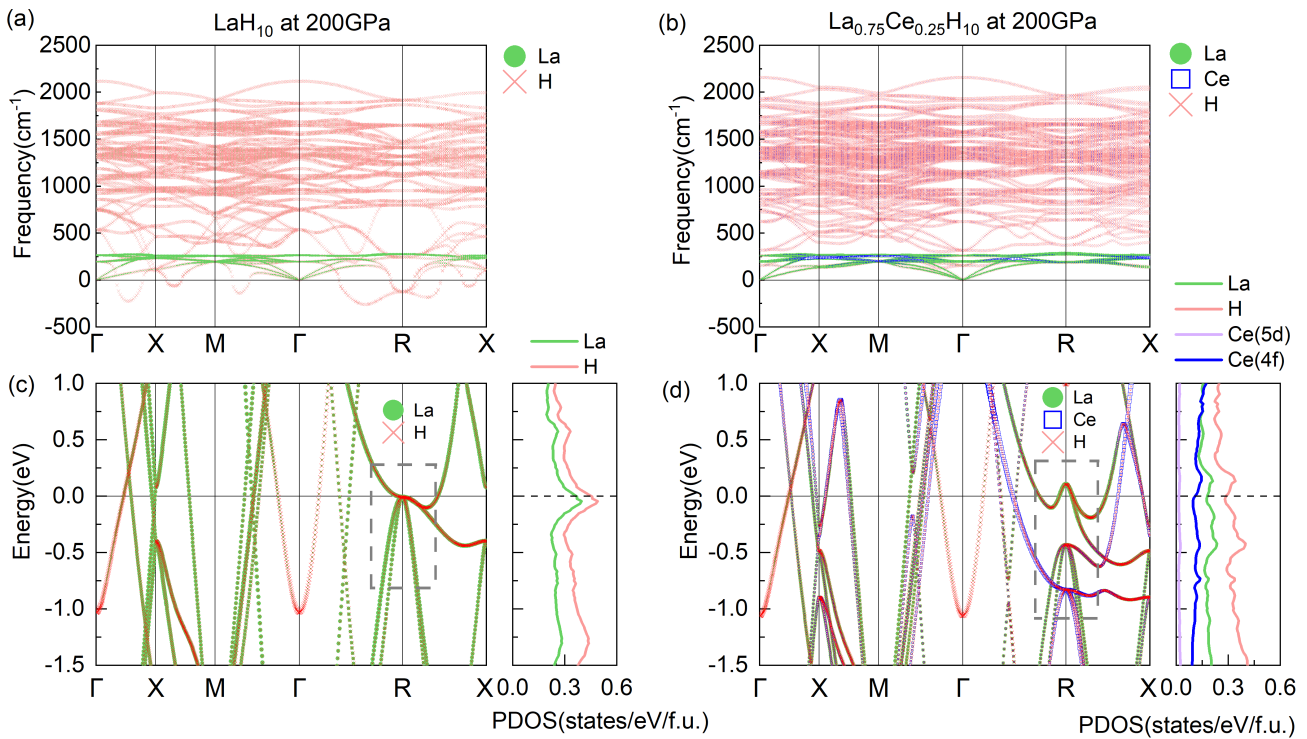


FIG. 3. (a) phonon dos of LaH<sub>10</sub> and La<sub>0.75</sub>Hf<sub>0.25</sub>H<sub>10</sub> at 400GPa. (b) and (c) Eliashberg spectrum function  $\alpha^2F(\omega)$ , and electron-phonon coupling integral  $\lambda(\omega)$  of LaH<sub>10</sub> and La<sub>0.75</sub>Hf<sub>0.25</sub>H<sub>10</sub> at 400GPa. (d) and (e) Phonon spectrum of LaH<sub>10</sub> and La<sub>0.75</sub>Hf<sub>0.25</sub>H<sub>10</sub> at 400GPa. The solid circles show the EPC with the area proportional to the respective phonon linewidth.

### 3.3 The effects of Ce

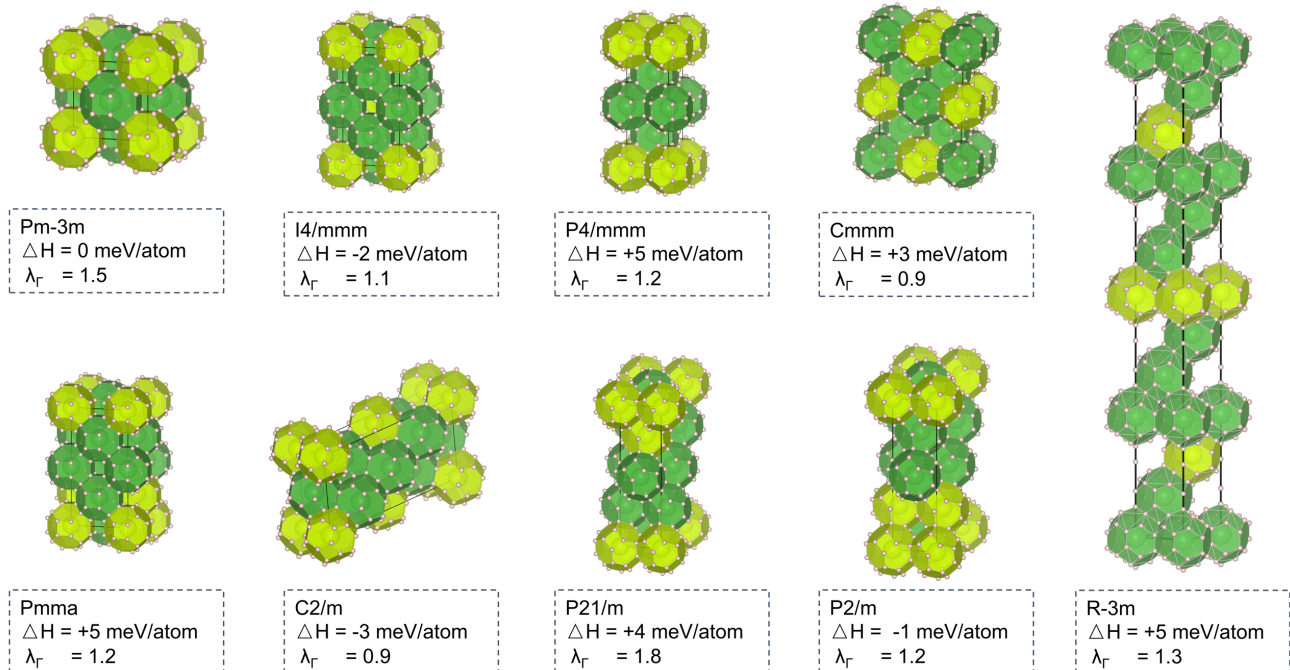
Ce is the only substitution that increases the pressure range of LaH<sub>10</sub> stability while maintaining the high-temperature superconductivity with a slight weakening of the EPC. To understand the effect of Ce substitution on dynamic stability, we compare the phonon spectrum between LaH<sub>10</sub> and

129 La<sub>0.75</sub>Ce<sub>0.25</sub>H<sub>10</sub> at 200 GPa in Fig. 4(a) and (b). In LaH<sub>10</sub>, the imaginary frequency modes on the  $\Gamma$ -X,  
 130  $\Gamma$ -M, and  $\Gamma$ -R paths are dominated by the vibrations of hydrogen atoms. When Ce is introduced, these  
 131 modes become stiffer, and the imaginary frequency disappears. In Fig. 4(c) and (d), we compare the  
 132 electronic band structure and density of states for LaH<sub>10</sub> and La<sub>0.75</sub>Ce<sub>0.25</sub>H<sub>10</sub>, respectively. LaH<sub>10</sub>  
 133 shows a flat band near the Fermi level with eightfold degeneracy at the **R** point. This caused a Van  
 134 Hove singularity (VHS) in the density of states. Ce substitution opens the gap at **R** and splits the  
 135 degenerated bands. This removes the VHS and reduces the states at the Fermi level. Correspondingly,  
 136 the imaginary modes at **R** disappear. Moreover, additional bands contributed mainly by Ce, and H  
 137 cross the Fermi level at  $\Gamma$ -M and  $\Gamma$ -R paths in La<sub>0.75</sub>Ce<sub>0.25</sub>H<sub>10</sub>. The bonding likely contributes to the  
 138 hardening of phonon modes. Based on the electronic density of states, these Ce bands near the Fermi  
 139 level are mostly from 4f orbitals. Therefore, this indicates that the 4f electron in Ce contributes  
 140 significantly to the dynamic stability of La<sub>0.75</sub>Ce<sub>0.25</sub>H<sub>10</sub>. To further validate this mechanism, we  
 141 computed the phonon spectrum of La<sub>0.75</sub>Ce<sub>0.25</sub>H<sub>10</sub> with the ultrasoft pseudopotential where Ce's 4f  
 142 electrons are regarded as core electrons. As shown in Supplementary Fig. 6, this ultrasoft  
 143 pseudopotential leads to the re-appearance of imaginary modes in La<sub>0.75</sub>Ce<sub>0.25</sub>H<sub>10</sub>, suggesting the  
 144 strong effect of 4f electrons in stabilizing the LaH<sub>10</sub> at low pressures.



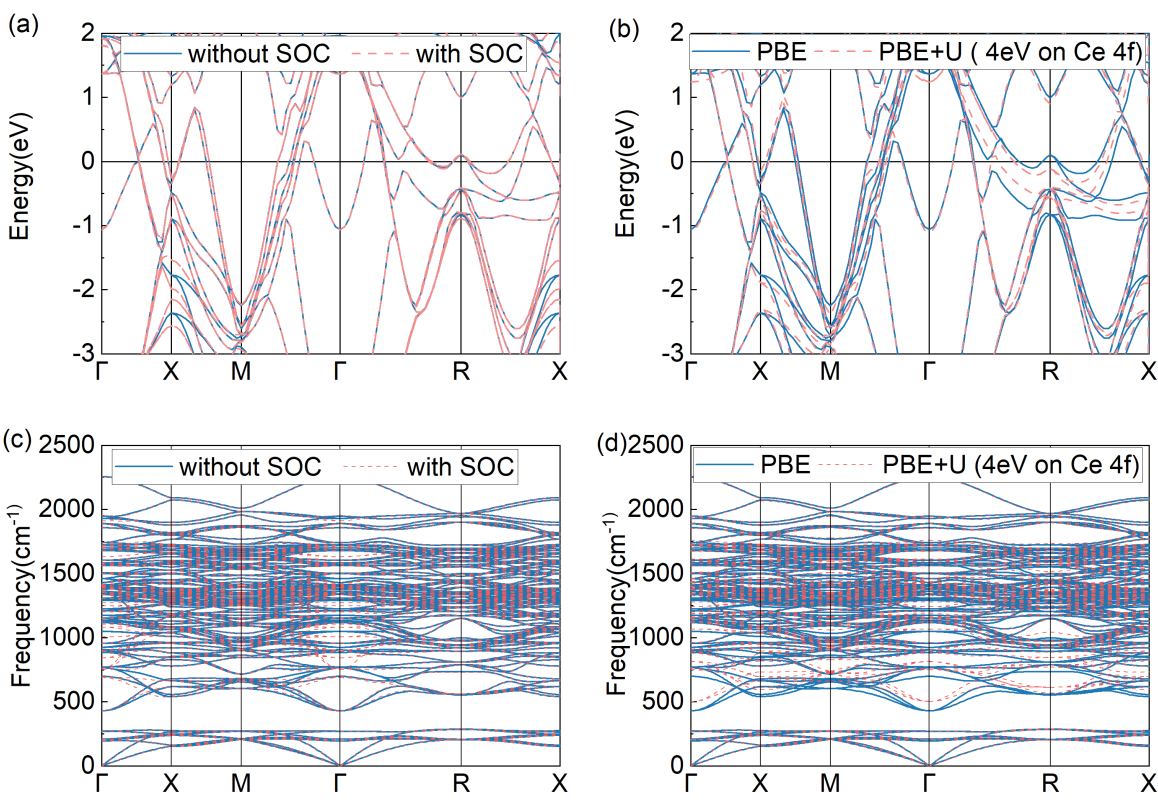
145  
 146 FIG. 4. (a) (b) Atom-projected phonon spectrum of LaH<sub>10</sub> and La<sub>0.75</sub>Ce<sub>0.25</sub>H<sub>10</sub> at 200GPa. (c) (d) fat  
 147 electron band (and projected density of states, PDOS) of LaH<sub>10</sub> and La<sub>0.75</sub>Ce<sub>0.25</sub>H<sub>10</sub> at 200GPa.

148 So far, the substitutional effect of Ce was only considered with Pm-3m  $\text{La}_{0.75}\text{Ce}_{0.25}\text{H}_{10}$  structure.  
 149 We further examine the stability of other  $\text{La}_{0.75}\text{Ce}_{0.25}\text{H}_{10}$  polymorphs at 200 GPa. As shown in Fig. 5,  
 150 we construct  $\text{LaH}_{10}$  supercells (88 atoms) by  $2 \times 2 \times 2$ ,  $1 \times 1 \times 8$  and  $1 \times 2 \times 4$  and randomly  
 151 replace La atoms with Ce atoms to generate 9 unique structures. Energy calculations show that these  
 152 structures all have similar enthalpy with differences of less than 5 meV/atom. To explore the possible  
 153 superconductivity in these structures, we employ a recently developed frozen-phonon method to  
 154 compute the zone-center EPC strength in the present structures. This efficient method can identify  
 155 strong EPC candidates in hydrides because the zone-center EPC strongly correlates with the full  
 156 Brillouin zone EPC in these materials [52]. Using this method, we compute the zone-center EPC,  $\lambda_{\Gamma}$ ,  
 157 for all the polymorphs. As shown in Fig. 5, different structures show similar  $\lambda_{\Gamma}$  as the one of the Pm-  
 158 3m phase. Therefore, Ce occupation in the  $\text{La}_{0.75}\text{Ce}_{0.25}\text{H}_{10}$  does not affect its energetic stability and  
 159 EPC. To confirm, we performed DFPT calculations of full Brillouin zone EPC for the P4/mmm phase  
 160 (see details in Fig. S7). We obtained  $\lambda$  of P4/mmm as 2.64, slightly smaller than the Pm-3m phase  
 161 ( $\lambda=3.08$ ). This is consistent with the zone-center EPC calculations. Furthermore, we used the  
 162 McMillan-Allen-Dynes formula and found the  $T_c$  of P4/mmm phase is 195K at 200GPa, which is  
 163 slightly smaller than the one of Pm-3m phase (224K). Since these polymorphs have similar enthalpy,  
 164 they may form a random solid solution in the experimental synthesis. Nevertheless, such a mixture  
 165 should maintain the HTS because of the similar electron-phonon coupling strength in these phases.



166  
 167 Fig. 5. The crystal structure, relative enthalpy and zone-center EPC of  $\text{La}_{0.75}\text{Ce}_{0.25}\text{H}_{10}$  polymorphs at  
 168 200GPa.

169 Additional effects such as spin-orbit coupling (SOC) and electron correlation of *f*-electron in Ce  
 170 may affect superconductivity of  $\text{La}_{0.75}\text{Ce}_{0.25}\text{H}_{10}$ . However, calculating the EPC and  $T_c$  directly under  
 171 these effects is highly complex and sophisticated. Therefore, we performed additional SOC and  
 172 DFT+U calculations to understand their effect on the electronic band structure and phonon dispersion  
 173 spectrum instead of direct calculations of EPC. Here we choose the U (Ce-4*f*) value of 4 eV for the  
 174 PBE+U calculation [53]. As shown in Fig. 6, both SOC and DFT+U calculations result in electronic  
 175 and phonon band structures similar to the one without these effects. Therefore, we expect these effects  
 176 should be weak on the EPC of  $\text{La}_{0.75}\text{Ce}_{0.25}\text{H}_{10}$ .



177  
 178 Fig. 6 (a) (b) Electron band structure of  $\text{La}_{0.75}\text{Ce}_{0.25}\text{H}_{10}$  with or without SOC or U effects. (c) (d)  
 179 phonon spectrum, respectively.

#### 180 IV. CONCLUSIONS

181 In summary, based on first-principles calculations, we have investigated the effects of chemical doping  
 182 on phase stability and superconductivity in the  $\text{LaH}_{10}$  structure. By analyzing the phonon spectrum,  
 183 we demonstrated that most doping elements (K, Rb, Cs, Ca, Sr, Ba, Sc, Y, Ti, Zr, Hf, Lu, In, Tl) induce  
 184 the softening of the high-frequency phonon modes, thereby enhancing the EPC and improving  $T_c$ .  
 185 However, phonon softening also leads to dynamical instability, reducing the stable pressure range.

Unlike these dopants, Ce doping can expand the range of dynamical stability for LaH<sub>10</sub> at lower pressures. The analysis of the electronic structures revealed that Ce doping eliminates the VHS and reduces states at the Fermi level, stiffening a few imaginary modes in LaH<sub>10</sub> at low pressures. Utilizing the Eliashberg theory and McMillan-Allen-Dynes formula, we demonstrated that La<sub>0.75</sub>Ce<sub>0.25</sub>H<sub>10</sub> maintains the high-temperature superconductivity with a  $T_c$  of ~ 224K at 200GPa. Upon examining different polymorphs of La<sub>0.75</sub>Ce<sub>0.25</sub>H<sub>10</sub>, we show that different doping sites of Ce in the LaH<sub>10</sub> structure have a minor effect on the energetic stability and EPC. Our findings suggest Ce can be a promising dopant to stabilize LaH<sub>10</sub> at lower pressures while preserving its high-temperature superconductivity. The experimental verification of our prediction is highly desirable.

## Reference

- [1] A. P. Drozdov, M. I. Eremets, I. A. Troyan, V. Ksenofontov, and S. I. Shylin, Conventional superconductivity at 203 kelvin at high pressures in the sulfur hydride system, *Nature* **525**, 73 (2015).
- [2] A. P. Drozdov, P. P. Kong, V. S. Minkov, M. Tkacz, and M. I. Eremets, Superconductivity at 250 K in lanthanum hydride under high pressures, *Nature* **569**, 528 (2019).
- [3] M. Somayazulu, M. Ahart, A. K. Mishra, Z. M. Geballe, M. Baldini, Y. Meng, V. V. Struzhkin, and R. J. Hemley, Evidence for Superconductivity above 260 K in Lanthanum Superhydride at Megabar Pressures, *Phys. Rev. Lett.* **122**, 027001 (2019).
- [4] Z. Li, X. He, C. Zhang, X. Wang, S. Zhang, Y. Jia, S. Feng, K. Lu, J. Zhao, J. Zhang, B. Min, Y. Long, R. Yu, L. Wang, M. Ye, Z. Zhang, V. Prakapenka, S. Chariton, P. A. Ginsberg, J. Bass, S. Yuan, H. Liu, and C. Jin, Superconductivity above 200 K discovered in superhydrides of calcium, *Nat. Commun.* **13**, 2863 (2022).
- [5] L. Ma, K. Wang, Y. Xie, X. Yang, Y. Wang, M. Zhou, H. Liu, X. Yu, Y. Zhao, H. Wang, G. Liu, and Y. Ma, High-Temperature Superconducting Phase in Clathrate Calcium Hydride CaH<sub>6</sub> up to 215 K at a Pressure of 172 GPa, *Phys. Rev. Lett.* **128**, 167001 (2022).
- [6] W. Chen, D. V. Semenok, X. Huang, H. Shu, X. Li, D. Duan, T. Cui, and A. R. Oganov, High-Temperature Superconducting Phases in Cerium Superhydride with a  $T_c$  up to 115 K below a Pressure of 1 Megabar, *Phys. Rev. Lett.* **127**, 117001 (2021).
- [7] J. Bi, Y. Nakamoto, P. Zhang, K. Shimizu, B. Zou, H. Liu, M. Zhou, G. Liu, H. Wang, and Y. Ma, Giant enhancement of superconducting critical temperature in substitutional alloy (La,Ce)H(9), *Nat. Commun.* **13**, 5952 (2022).
- [8] W. Chen, X. Huang, D. V. Semenok, S. Chen, D. Zhou, K. Zhang, A. R. Oganov, and T. Cui, Enhancement of superconducting properties in the La-Ce-H system at moderate pressures, *Nat. Commun.* **14**, 2660 (2023).
- [9] P. Kong, V. S. Minkov, M. A. Kuzovnikov, A. P. Drozdov, S. P. Besedin, S. Mozaffari, L. Balicas, F. F. Balakirev, V. B. Prakapenka, S. Chariton, D. A. Knyazev, E. Greenberg, and M. I. Eremets, Superconductivity up to 243 K in the yttrium-hydrogen system under high pressure, *Nat. Commun.* **12**, 5075 (2021).
- [10] E. Snider, N. Dasenbrock-Gammon, R. McBride, X. Wang, N. Meyers, K. V. Lawler, E. Zurek, A. Salamat, and R. P. Dias, Synthesis of Yttrium Superhydride Superconductor with a Transition

- 226 Temperature up to 262 K by Catalytic Hydrogenation at High Pressures, Phys. Rev. Lett. **126**, 117003  
227 (2021).
- 228 [11] Y. Wang, K. Wang, Y. Sun, L. Ma, Y. Wang, B. Zou, G. Liu, M. Zhou, and H. Wang, Synthesis and  
229 superconductivity in yttrium superhydrides under high pressure, Chin. Phys. B **31**, 106201 (2022).
- 230 [12] Y. Song, J. Bi, Y. Nakamoto, K. Shimizu, H. Liu, B. Zou, G. Liu, H. Wang, and Y. Ma,  
231 Stoichiometric Ternary Superhydride LaBeH<sub>8</sub> as a New Template for High-Temperature  
232 Superconductivity at 110 K under 80 GPa, Phys. Rev. Lett. **130**, 266001 (2023).
- 233 [13] J. A. Flores-Livas, L. Boeri, A. Sanna, G. Profeta, R. Arita, and M. Eremets, A perspective on  
234 conventional high-temperature superconductors at high pressure: Methods and materials, Phys. Rep.  
235 **856**, 1 (2020).
- 236 [14] L. P. Gor'kov and V. Z. Kresin, Colloquium: High pressure and road to room temperature  
237 superconductivity, Rev. Mod. Phys. **90**, 011001 (2018).
- 238 [15] B. Lilia, R. Hennig, P. Hirschfeld, G. Profeta, A. Sanna, E. Zurek, W. E. Pickett, M. Amsler, R.  
239 Dias, M. I. Eremets, C. Heil, R. J. Hemley, H. Liu, Y. Ma, C. Pierleoni, A. N. Kolmogorov, N. Rybin,  
240 D. Novoselov, V. Anisimov, A. R. Oganov, C. J. Pickard, T. Bi, R. Arita, I. Errea, C. Pellegrini, R.  
241 Requist, E. K. U. Gross, E. R. Margine, S. R. Xie, Y. Quan, A. Hire, L. Fanfarillo, G. R. Stewart, J. J.  
242 Hamlin, V. Stanev, R. S. Gonnelli, E. Piatti, D. Romanin, D. Daghero, and R. Valenti, The 2021 room-  
243 temperature superconductivity roadmap, J. Phys. Condens. Matter **34**, 183002 (2022).
- 244 [16] C. J. Pickard, I. Errea, and M. I. Eremets, Superconducting Hydrides Under Pressure, Annu. Rev.  
245 Condens. Matter Phys. **11**, 57 (2020).
- 246 [17] W. E. Pickett, Colloquium: Room temperature superconductivity: The roles of theory and  
247 materials design, Rev. Mod. Phys. **95**, 021001 (2023).
- 248 [18] Y. Sun, H.-Y. Liu, and Y.-M. Ma, Progress on hydrogen-rich superconductors under high pressure,  
249 Acta Physica Sinica **70**, 017407 (2021).
- 250 [19] M. Du, W. Zhao, T. Cui, and D. Duan, Compressed superhydrides: the road to room temperature  
251 superconductivity, J Phys Condens Matter **34**, 173001 (2022).
- 252 [20] D. V. Semenok, I. A. Kruglov, I. A. Savkin, A. G. Kvashnin, and A. R. Oganov, On Distribution  
253 of Superconductivity in Metal Hydrides, Curr. Opin. Solid State Mater. Sci. **24**, 100808 (2020).
- 254 [21] X. Zhang, Y. Zhao, and G. Yang, Superconducting ternary hydrides under high pressure, Wiley  
255 Interdisciplinary Reviews: Computational Molecular Science **12**, e1582 (2021).
- 256 [22] Z. Zhang, T. Cui, M. J. Hutcheon, A. M. Shipley, H. Song, M. Du, V. Z. Kresin, D. Duan, C. J.  
257 Pickard, and Y. Yao, Design Principles for High-Temperature Superconductors with a Hydrogen-Based  
258 Alloy Backbone at Moderate Pressure, Phys. Rev. Lett. **128**, 047001 (2022).
- 259 [23] M. Gao, X.-W. Yan, Z.-Y. Lu, and T. Xiang, Phonon-mediated high-temperature superconductivity  
260 in the ternary borohydride KB<sub>2</sub>H<sub>8</sub> under pressure near 12 GPa, Phys. Rev. B **104**, L100504 (2021).
- 261 [24] S. Di Cataldo, W. von der Linden, and L. Boeri, First-principles search of hot superconductivity  
262 in La-X-H ternary hydrides, npj Comput. Mater **8**, 2 (2022).
- 263 [25] S. Di Cataldo, C. Heil, W. von der Linden, and L. Boeri, LaBH<sub>8</sub>: Towards high-Tc low-pressure  
264 superconductivity in ternary superhydrides, Phys. Rev. B **104**, L020511 (2021).
- 265 [26] N. Geng, K. P. Hilleke, L. Zhu, X. Wang, T. A. Strobel, and E. Zurek, Conventional High-  
266 Temperature Superconductivity in Metallic, Covalently Bonded, Binary-Guest C-B Clathrates, J. Am.  
267 Chem. Soc. **145**, 1696 (2023).
- 268 [27] Y. Hai, H. Tian, M. Jiang, W. Li, G. Zhong, C. Yang, X. Chen, and H. Lin, Improving Tc in

- 269 sodalite-like boron-nitrogen compound M<sub>2</sub>(BN)6, Mater. Today Phys. **25**, 100699 (2022).
- 270 [28] R. Wang, Y. Sun, S. Wu, V. Antropov, and K. M. Ho, High-Throughput Screening of Strong  
271 Electron-Phonon Couplings in Ternary Metal Diborides, Inorg. Chem. **61**, 18154 (2022).
- 272 [29] M. Du, H. Song, Z. Zhang, D. Duan, and T. Cui, Room-Temperature Superconductivity in Yb/Lu  
273 Substituted Clathrate Hexahydrides under Moderate Pressure, Research **2022**, 9784309 (2022).
- 274 [30] Y.-L. Hai, H.-L. Tian, M.-J. Jiang, H.-B. Ding, Y.-J. Feng, G.-H. Zhong, C.-L. Yang, X.-J. Chen,  
275 and H.-Q. Lin, Prediction of high-T<sub>c</sub> superconductivity in H<sub>6</sub>SX(X=Cl,Br) at pressures below one  
276 megabar, Phys. Rev. B **105**, L180508 (2022).
- 277 [31] M.-J. Jiang, Y.-L. Hai, H.-L. Tian, H.-B. Ding, Y.-J. Feng, C.-L. Yang, X.-J. Chen, and G.-H.  
278 Zhong, High-temperature superconductivity below 100GPa in ternary C-based hydride MC<sub>2</sub>H<sub>8</sub> with  
279 molecular crystal characteristics ( M= Na, K, Mg, Al, and Ga), Phys. Rev. B **105**, 104511 (2022).
- 280 [32] T. Wang, J. A. Flores-Livas, T. Nomoto, Y. Ma, T. Koretsune, and R. Arita, Optimal alloying in  
281 hydrides: Reaching room-temperature superconductivity in LaH<sub>10</sub>, Phys. Rev. B **105**, 174516 (2022).
- 282 [33] H. Song, Z. Zhang, T. Cui, C. J. Pickard, V. Z. Kresin, and D. Duan, High T<sub>c</sub> Superconductivity  
283 in Heavy Rare Earth Hydrides, Chin. Phys. Lett. **38**, 107401 (2021).
- 284 [34] X. Zhong, Y. Sun, T. Iitaka, M. Xu, H. Liu, R. J. Hemley, C. Chen, and Y. Ma, Prediction of Above-  
285 Room-Temperature Superconductivity in Lanthanide/Actinide Extreme Superhydrides, J. Am. Chem.  
286 Soc. **144**, 13394 (2022).
- 287 [35] J. P. Perdew, K. Burke, and M. Ernzerhof, Generalized gradient approximation made simple, Phys.  
288 Rev. Lett. **77**, 3865 (1996).
- 289 [36] P. E. Blochl, Projector augmented-wave method, Phys. Rev. B **50**, 17953 (1994).
- 290 [37] G. Kresse and J. Furthmüller, Efficient iterative schemes for ab initio total-energy calculations  
291 using a plane-wave basis set, Phys. Rev. B **54**, 11169 (1996).
- 292 [38] S. Baroni, S. De Gironcoli, A. Dal Corso, and P. Giannozzi, Phonons and related crystal properties  
293 from density-functional perturbation theory, Rev. Mod. Phys. **73**, 515 (2001).
- 294 [39] P. Giannozzi, O. Andreussi, T. Brumme, O. Bunau, M. Buongiorno Nardelli, M. Calandra, R. Car,  
295 C. Cavazzoni, D. Ceresoli, M. Cococcioni, N. Colonna, I. Carnimeo, A. Dal Corso, S. de Gironcoli, P.  
296 Delugas, R. A. DiStasio, Jr., A. Ferretti, A. Floris, G. Fratesi, G. Fugallo, R. Gebauer, U. Gerstmann,  
297 F. Giustino, T. Gorni, J. Jia, M. Kawamura, H. Y. Ko, A. Kokalj, E. Kucukbenli, M. Lazzeri, M. Marsili,  
298 N. Marzari, F. Mauri, N. L. Nguyen, H. V. Nguyen, A. Otero-de-la-Roza, L. Paulatto, S. Ponce, D.  
299 Rocca, R. Sabatini, B. Santra, M. Schlipf, A. P. Seitsonen, A. Smogunov, I. Timrov, T. Thonhauser, P.  
300 Umari, N. Vast, X. Wu, and S. Baroni, Advanced capabilities for materials modelling with Quantum  
301 ESPRESSO, J. Phys. Condens. Matter **29**, 465901 (2017).
- 302 [40] P. Giannozzi, S. Baroni, N. Bonini, M. Calandra, R. Car, C. Cavazzoni, D. Ceresoli, G. L. Chiarotti,  
303 M. Cococcioni, I. Dabo, A. Dal Corso, S. de Gironcoli, S. Fabris, G. Fratesi, R. Gebauer, U. Gerstmann,  
304 C. Gougaussis, A. Kokalj, M. Lazzeri, L. Martin-Samos, N. Marzari, F. Mauri, R. Mazzarello, S.  
305 Paolini, A. Pasquarello, L. Paulatto, C. Sbraccia, S. Scandolo, G. Sclauzero, A. P. Seitsonen, A.  
306 Smogunov, P. Umari, and R. M. Wentzcovitch, QUANTUM ESPRESSO: a modular and open-source  
307 software project for quantum simulations of materials, J. Phys. Condens. Matter **21**, 395502 (2009).
- 308 [41] A. Dal Corso, Pseudopotentials periodic table: From H to Pu, Comput. Mater. Sci. **95**, 337 (2014).
- 309 [42] P. B. Allen and R. C. Dynes, Transition temperature of strong-coupled superconductors reanalyzed,  
310 Phys. Rev. B **12**, 905 (1975).
- 311 [43] W. L. McMillan, Transition Temperature of Strong-Coupled Superconductors, Phys. Rev. **167**, 331

- 312 (1968).
- 313 [44]H. Liu, Naumov, II, R. Hoffmann, N. W. Ashcroft, and R. J. Hemley, Potential high-T(c)  
314 superconducting lanthanum and yttrium hydrides at high pressure, Proc. Natl. Acad. Sci. U.S.A. **114**,  
315 6990 (2017).
- 316 [45]P. Morel and P. W. Anderson, Calculation of the Superconducting State Parameters with Retarded  
317 Electron-Phonon Interaction, Phys. Rev. **125**, 1263 (1962).
- 318 [46]I. Errea, F. Belli, L. Monacelli, A. Sanna, T. Koretsune, F. Mauri, and J. A. Flores-Livas, Quantum  
319 crystal structure in the 250-kelvin superconducting lanthanum hydride, Nature **578**, 66 (2020).
- 320 [47]D. Sun, V. S. Minkov, S. Mozaffari, L. Balicas, and F. F. Balakirev, High-temperature  
321 superconductivity on the verge of a structural instability in lanthanum superhydride, Nat. Commun.  
322 **12**, 6863 (2021).
- 323 [48]P. B. Allen and M. L. Cohen, Superconductivity and Phonon Softening, Phys. Rev. Lett. **29**, 1593  
324 (1972).
- 325 [49]P. B. Allen and R. C. Dynes, Superconductivity and phonon softening: II. Lead alloys, Phys. Rev.  
326 B **11**, 1895 (1975).
- 327 [50]K. Kudo, M. Takasuga, Y. Okamoto, Z. Hiroi, and M. Nohara, Giant phonon softening and  
328 enhancement of superconductivity by phosphorus doping of BaNi<sub>2</sub>As<sub>2</sub>, Phys. Rev. Lett. **109**, 097002  
329 (2012).
- 330 [51]W. E. Pickett and P. B. Allen, Superconductivity and phonon softening. III. Relation between  
331 electron bands and phonons in Nb, Mo, and their alloys, Phys. Rev. B **16**, 3127 (1977).
- 332 [52]Y. Sun, F. Zhang, C.-Z. Wang, K.-M. Ho, I. I. Mazin, and V. Antropov, Electron-phonon coupling  
333 strength from ab initio frozen-phonon approach, Phys. Rev. Mater. **6**, 074801 (2022).
- 334 [53]B. Y. Ao, X. L. Wang, P. Shi, P. H. Chen, X. Q. Ye, X. C. Lai, J. J. Ai, and T. Gao, Lattice  
335 contraction of cerium hydrides from first-principles LDA+U calculations, Int. J. Hydrogen Energy **37**,  
336 5108 (2012).
- 337

### 338 Acknowledgements

339 Y.S. acknowledges support from the Fundamental Research Funds for the Central Universities  
340 (20720230014). V.P. was supported by the U.S. Department of Energy, Office of Basic Energy  
341 Sciences, Division of Materials Sciences and Engineering. Ames National Laboratory is operated for  
342 the U.S. Department of Energy by Iowa State University under Contract No. DE-AC02-07CH11358.  
343 K.M.H. acknowledges support from National Science Foundation Awards No. DMR-2132666. S. Fang  
344 and T. Wu from Information and Network Center of Xiamen University are acknowledged for the help  
345 with the GPU computing. Tan Kah Kee Supercomputing Center is acknowledged for the support of  
346 high-performance computing.